Surface and bulk electronic structure of aluminium diboride

V. Sunko [1,2,*] D. Milosavljević,[1] F. Mazzola,[2] O. J. Clark,[2] U. Burkhardt,[1] T. K. Kim [3] H. Rosner,[1] Yu. Grin,[1]
A. P. Mackenzie,[1,2] and P. D. C. King[2,†]

[1]*Max Planck Institute for Chemical Physics of Solids, Nöthnitzer Straße 40, 01187 Dresden, Germany*
[2]*SUPA, School of Physics and Astronomy, University of St Andrews, St Andrews KY16 9SS, United Kingdom*
[3]*Diamond Light Source, Harwell Campus, Didcot OX11 0DE, United Kingdom*

We report a combined experimental and theoretical study of the surface and bulk electronic structure of aluminium diboride, a nonsuperconducting sister compound of the superconductor MgB_2. We perform angle-resolved photoemission measurements with variable photon energy, and compare them to density functional theory calculations to disentangle the surface and bulk contributions to the measured spectra. Aluminium diboride is known to be aluminium deficient, $Al_{1-\delta}B_2$, which would be expected to lead to a hole doping as compared to the nominally stoichimoetric compound. Nonetheless, we find that the bulk σ states, which mediate superconductivity in MgB_2, remain more than 600 meV below the Fermi level. However, we also observe σ states originating from the boron terminated surface, with an order of magnitude smaller binding energy of 70 meV, and demonstrate how surface hole-doping can bring these across the Fermi level.

I. INTRODUCTION

Magnesium diboride (MgB_2) has the highest critical temperature, $T_c = 39$ K, of any known "conventional," i.e., phonon-mediated, superconductor at ambient pressure [1]. The superconductivity originates from partially occupied σ bands of its graphene-like boron layers, and it is mediated by a large electron-phonon coupling between the electrons occupying those bands and the high-frequency phonons associated with the in-plane vibration of boron atoms. This strong coupling arises as a consequence of the in-plane charge distribution of the σ-states that is asymmetric with respect to the boron lattice positions [2], motivating the study of other systems containing hexagonal networks of boron atoms. One such material is AlB_2, which is isostructural with MgB_2 [Fig. 1(a)]. Comparing the number of valence electrons available from the two metals (two for Mg, three for Al), the boron layer in AlB_2 may be understood as an electron-doped version of that in MgB_2. Density functional theory (DFT) calculations predict that this electron doping fills the σ bands and moves the Fermi level far above them [3], and is therefore detrimental to superconductivity.

There are, however, reasons why the σ states may be located closer to E_F than expected from calculations. First, there are known issues related to the stoichiometry of aluminium

diboride: the most thorough chemical analysis reveals that even crystals grown in Al-rich conditions are Al-deficient, yielding a composition of $Al_{0.9}B_2$ [4]. Also, first principles calculations show that the Al-deficient composition is more stable than stoichiometric AlB_2 [5]. We therefore refer to aluminium diboride as $Al_{1-\delta}B_2$ to reflect the aluminium deficiency, which makes the electron count in the B-layers of the real material more similar to the electron count in the B-layers of MgB_2 than to that in stoichiometric AlB_2. While it is known that $Al_{1-\delta}B_2$ is not superconducting [4,6], the energy of its σ bands with respect to the Fermi level has not been established. This is an important question because if their binding energy is small enough it may be possible to utilize external tuning, such as uniaxial pressure, or deliberate carrier doping, to drive the σ states through the Fermi level. This would provide a potential route to inducing superconductivity. Rather than creating "just" a slightly modified version of the MgB_2 case, however, such an experiment would provide the exciting opportunity to continuously tune the density of σ states at the Fermi level, in turn offering a high degree of control over the superconducting properties and parameters [7]; it would possibly even create the ability to tune between weak- and strong-coupling regimes [8,9].

Moreover, the charged nature of the individual layers of $Al_{1-\delta}B_2$ leads to its (001) surfaces being polar. The (001) surfaces therefore have to undergo either a structural or an electronic reconstruction to neutralize the surface charge [10]. The simplest route to achieving this is a charge redistribution, whereby the layers which are negatively (positively) charged in the bulk become hole-doped (electron-doped) with respect to their bulk versions when they are found on surfaces; this mechanism is known to account for surface features in other layered compounds with polar surfaces [11–14]. Specifically, this means that if the B-terminated surface of $Al_{1-\delta}B_2$ preserved the bulk composition and structure, the surface states

*veronika.sunko@cpfs.mpg.de
†pdk6@st-andrews.ac.uk

localized on it could resemble a hole-doped version of their bulk counterpart, i.e., the surface σ states could cross the Fermi level, offering a potential platform for creating two-dimensional surface superconductivity, which may also be controllable by external tuning. This prospect is particularly intriguing in the context of recent theoretical predictions of multigap superconductivity in thin films of AlB_2 [15].

The main goal of this paper is thus to determine whether either bulk or surface σ bands of $Al_{1-\delta}B_2$ cross the Fermi level, or are close enough to it that they could be tuned across it by doping or other external perturbations. This requires an experimental approach, as it is difficult to characterize the disorder caused by the aluminium off-stoichiometry, and to reliably theoretically investigate its influence on the electronic band structure. Angle-resolved photoemission spectroscopy (ARPES) is the ideal tool to address these questions, as it provides information on the momentum- and energy-resolved spectral function, and it is sensitive to both the surface and bulk electronic structure [16]. Here we report on photon-energy dependent ARPES measurements of $Al_{1-\delta}B_2$ single crystals, which we use to disentangle the bulk and surface contributions to the measured ARPES spectra. We compare them to the DFT calculations of the surface and bulk electronic structure of stoichiometric AlB_2, and use this comparison to aid attribution of the observed features. We find that the bulk σ states have their band top located 0.6 eV below the Fermi level, and it is therefore not likely that they can be tuned across it. In contrast, the surface σ states originating from the B-terminated surface are much closer to the Fermi level, and we demonstrate how they can be driven across it by surface doping, indicating a promising avenue for future research.

This paper is organized as follows. In Sec. II we introduce the experimental and theoretical methods used in this study. In Sec. III A we describe the bulk electronic structure of stoichiometric AlB_2, as calculated by DFT, while in Sec. III B we discuss the surface electronic structure, calculated for both the B- and the Al-terminated surface of AlB_2. We use this information to help identify the states observed in the ARPES experiments whose results are reported in Sec. IV. Finally, in Sec. V we discuss the possibility of tuning these states across the Fermi level, and demonstrate that this is indeed possible for boron-derived surface states.

II. METHODS

To prepare the aluminium diboride single crystals an Al-rich mixture (97.7% Al, 2.3% B) of high purity aluminium and boron was melted in a furnace under argon atmosphere using alumina crucibles. The melt was slowly cooled during 18 hours from 1350° C to 660° C, and the excess aluminium was dissolved in a diluted hydrochloric acid. The obtained crystals are truncated or complete hexagonal plates with lateral dimensions on the order of a millimeter and several micrometer thickness along the c-axis. More details of the sample preparation and characterization are given in Ref. [4].

ARPES measurements were performed at the I05 beamline of Diamond Light Source, using a Scienta R4000 hemispherical electron analyzer [17]. The manipulator temperature was held at $\sim$6 K. We used linear horizontal (LH, p-polarized)

photons for all the measurements, with the photon energy ranging between 50 and 130 eV.

Relativistic density functional (DFT) electronic structure calculations have been carried out using the full-potential local-orbital basis (FPLO) code [18], version FPLO18.00-52. The exchange correlation potential was treated in the local density approximation (LDA) using the Perdew-Wang parametrization [19]. For the bulk electronic structure, we also performed calculations using the general gradient approximation (GGA) as the exchange correlation potential [20]. LDA and GGA yield no significant differences for the valence band. All the calculations were carried out using the experimental room temperature crystal structure with the lattice parameters of $a = 3.0050(1)$ Å and $c = 3.2537(8)$ Å [4]. For the bulk calculations, a well-converged k mesh of $12 \times 12 \times 12$ k-points in the whole Brillouin zone was employed (1728 in the whole and 133 in the irreducible wedge of the Brillouin zone). To calculate the electronic structure of the two surface terminations we constructed symmetric slabs, containing 15 Al layers for the B-terminated slabs ($Al_{15}B_{32}$) and 14 B layers for the Al-terminated slabs ($Al_{15}B_{28}$). Inversion symmetric slabs are used to avoid the formation of permanent electrical dipoles arising from the surface charge, and to therefore ensure the convergence and high accuracy of the calculated band dispersions. However, such slabs require a stoichiometry slightly different from that of the bulk. While this off-stoichiometry necessarily influences the calculated Fermi level, it is not expected to change the band dispersion. We therefore compare the dispersions of calculated and measured surface bands, but not their energies referenced to the Fermi level. The vacuum spacing between consecutive slabs along the z direction was larger than 13 Å in both calculations, large enough to avoid any interaction between the slabs. Starting from the ideal truncated bulk crystal structure, surface and subsurface atomic positions of both slab terminations were relaxed with respect to the total energy, yielding no significant changes in the band structure. Corresponding to the bulk calculations, a k-mesh of $12 \times 12 \times 2$ k-points was used.

III. DENSITY FUNCTIONAL THEORY CALCULATIONS

A. Bulk states

The crystal structure of AlB_2 consists of alternating layers of boron and aluminium atoms [space group $P6/mmm$, Fig. 1(a)], with a corresponding hexagonal bulk Brillouin zone [Fig. 1(b)]. The electronic structure in the energy range shown in Fig. 1(c) (-15 to 2 eV) is dominated by boron-derived states [orange in Fig. 1(c)], which form bands resembling those of graphene. Indeed, bands corresponding to the σ and π states, composed of sp^2 hybrid orbitals and p_z orbitals, respectively, can be identified, and are labeled in Fig. 1(c). The doubly degenerate band top of the σ bands at the Γ point is found 1.8 eV below the Fermi level, while the Dirac cone formed by the π states at the K point is situated 0.17 eV above the Fermi level. In contrast to graphene, however, the σ and π states derived from the boron orbitals in AlB_2 can, and do, disperse in the out-of-plane direction. Consequently, the energy of the top of the σ bands changes by 0.7 eV between the Γ and A points [Fig. 1(b)], reaching -1.1 eV at the A point
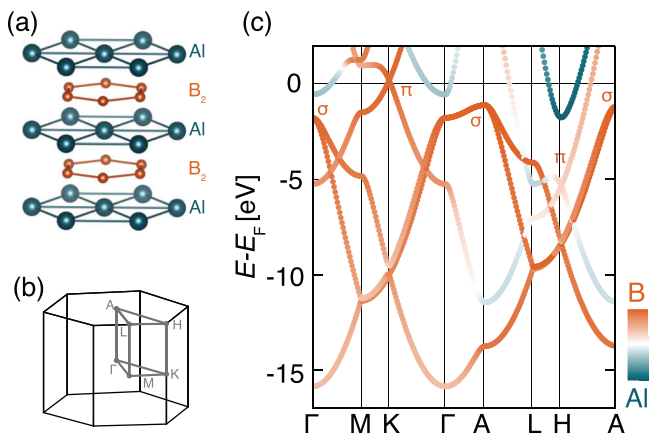
FIG. 1. (a) Crystal structure and the (b) bulk Brillouin zone of AlB_2. (c) The electronic structure of AlB_2 calculated by DFT, and colored according to the atomic character of the wave function.

[Fig. 1(c)]. This degree of out-of-plane dispersion is larger than in MgB_2, in which the energy of the σ state band top changes by about 0.4 eV between the Γ and A points [21], reflecting the smaller c/a ratio in AlB_2.

Unsurprisingly, the π states formed by the out-of-plane p_z orbitals disperse even more along the out-of-plane direction. At the H point, the Dirac crossing is found 5.4 eV below the Fermi level, i.e., its energy changes by more than 5.5 eV between the K and H points of the Brillouin zone. A Dirac-like crossing occurs at the Brillouin zone corner for each value of the out-of-plane momentum, thus forming a so-called Dirac nodal line along the K–H direction, which has recently been experimentally observed using soft x-ray ARPES [22]. Furthermore, the three-dimensional nature of the p_z orbitals enables a larger degree of hybridization with the Al orbitals. Consequently, the orbital composition changes along K–H: the boron orbitals contribute 96% of the wave-function weight at the K–H point Dirac crossing, and only 63% at the K–H
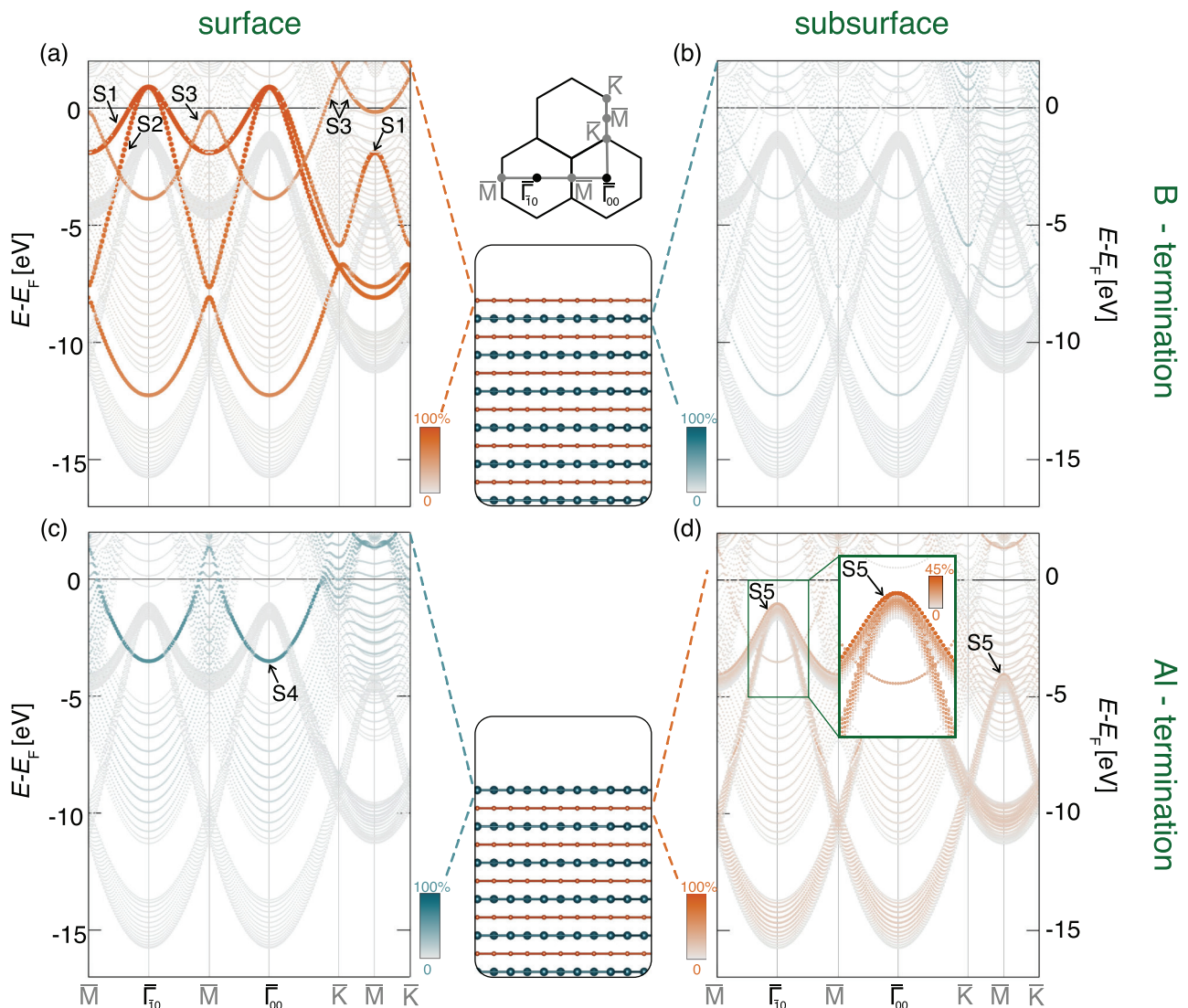

FIG. 2. DFT electronic structure of (a), (b) B—terminated and (c), (d) Al—terminated slabs of AlB_2. The color and size of the symbols show the wave-function projection on surface and subsurface layers: (a) surface B and (b) subsurface Al for the B-terminated slab; (c) surface Al and (d) subsurface B for the Al-terminated slab. The labels S1-S5 are explained in the text.

point. In contrast, for the top of the σ bands the boron contribution only changes between 98% and 100% between the Γ and A points.

As well as those states dominated by the boron orbitals, additional three-dimensional states are visible in the vicinity of the Fermi level around the Γ and H points of the Brillouin zone. These have a significant aluminium contribution.

B. Surface states

As discussed above, the polar nature of the surface may lead to a markedly modified surface environment as compared to the bulk. For a typical cleaved surface, both B-terminated and Al-terminated regions are expected with equal probability, thus yielding signatures of both surfaces in a typical ARPES experiment. To guide the interpretation of those experiments, we show the calculated electronic structure of B- [Figs. 2(a) and 2(b)] and Al-terminated [Figs. 2(c) and 2(d)] AlB$_2$ su-percells. We show the calculations over an extended and repeated k-space path (inset of Fig. 2) to facilitate comparison of the calculations with the ARPES results shown below, where intensity variations are present due to matrix element variations which do not follow the basic periodicity of the solid.

First we describe the signatures of the B-terminated surface, whose band structure is shown coloured according to the wave function weight of the surface B layer and the subsurface Al layer, respectively, in Figs. 2(a) and 2(b). Four bands whose character derives almost entirely from the surface B atoms are visible in the energy window shown in Fig. 2. These correspond to three states formed by the sp^2 hybrid orbitals (i.e., σ states) and one formed by the p_z orbital (i.e., the π state), in direct analogy with graphene. The lowest-lying σ state is found $\sim$10 eV below the Fermi level, and we do not consider it further here. The remaining two σ states and the π state all cross the Fermi level in our calculations, consistent with simple ionic argument stating that a layer charged nega-tively in the bulk becomes hole-doped with respect to its bulk version [cf. Fig. 1(c)] at the surface. We label these σ states as S1 and S2, and the π state as S3 [Fig. 2(a)]. In contrast to the rich electronic structure of the B surface layer, the subsurface Al layer is not expected to contribute significantly to the electronic structure in this energy window [Fig. 2(b)].

In Figs. 2(c) and 2(d) we show the band structure of the Al-terminated slab, colored by the wave-function weight of the surface Al layer and the subsurface B layer, respectively. The surface Al layer supports a single, electron-like band centered at the $\overline{\Gamma}$ point (labelled S4), which corresponds to an electron-doped surface copy of the Al-dominated bulk state visible at the Γ point in Fig. 1(c). An additional surface state is also visible which has a significant wave-function weight on the subsurface B layer. This state, labeled S5, and seen most clearly in the inset of Fig. 2(d), dominantly follows the highest occupied bulk σ band [Fig. 2(d)]. It resembles the surface state S1 of the boron termination [Fig. 2(a)], but with a higher binding energy. While the subsurface B layer contributes the largest fraction of the wave-function weight of this state (42%), it also has a significant weight on boron atoms in layers deeper in the material: 34% stems from second boron layer, 15% from the third, 6% from the fourth,
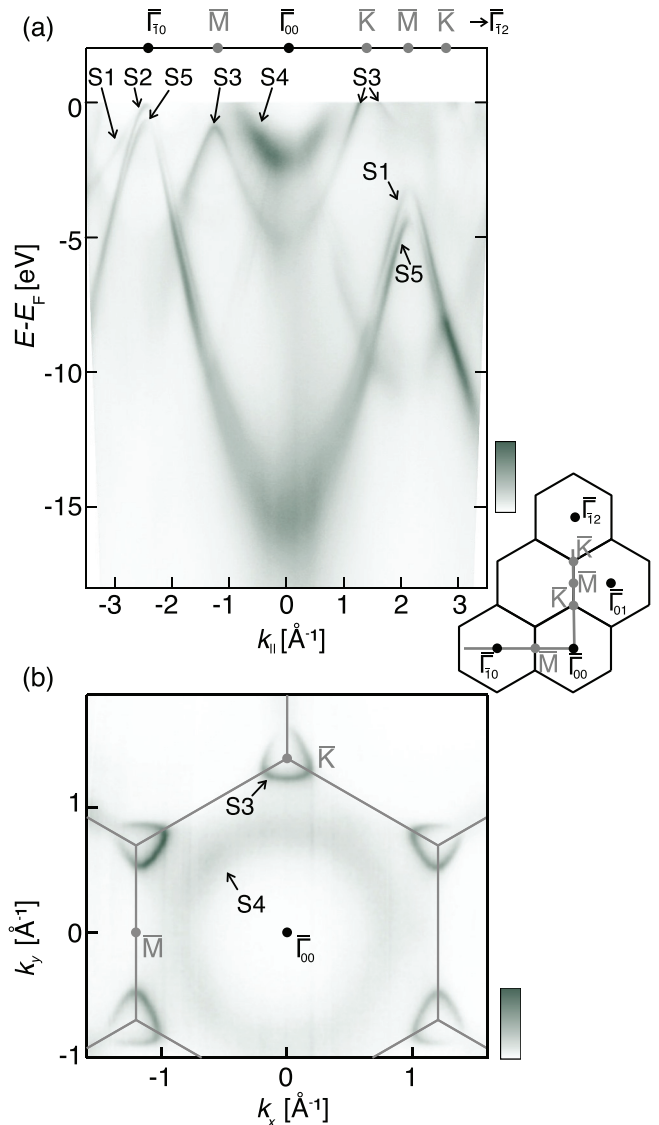

FIG. 3. (a) Electronic structure measured along the k-space path indicated in the inset, and (b) the Fermi surface ($E_F \pm$ 100 meV) of AlB$_2$, measured by ARPES ($h\nu = 118$ eV, p-pol).

and about 3% from the remaining boron layers. This greater wave-function extension into the bulk reflects that the state is not dispersing in a projected surface band gap, but rather is nearly degenerate with the k_z-projected bulk σ states.

In total, therefore, the calculations predict five two-dimensional states in the vicinity of the Fermi level, across the two surface terminations. Three of them have the character of boron σ bands (S1, S2, S5), one of a boron π band (S3), and one is an electron-like pocket of Al character (S4). In the following section we will experimentally identify these states.

IV. EXPERIMENTAL RESULTS

A. In-plane electronic structure

In Fig. 3(a) we show an ARPES measurement of Al$_{1-\delta}$B$_2$, taken along the same path (inset) as the calculations shown in Fig. 2. The ARPES intensity does not follow the periodicity of the surface Brillouin zone: the spectra measured at the $\overline{\Gamma}_{00}$

and $\overline{\Gamma}_{\overline{1}0}$ points are strikingly different, as are those measured at the two $\overline{\mathrm{M}}$ points shown in Fig. 3(a). This is a known matrix element effect, originating from the marked anisotropy of the sp^2 orbitals, which is well documented in graphene [23]. We therefore do not discuss it further here, but show our measurements over an extended k-space path to ensure visibility of the relevant band-structure features.

Three bands are observed in the vicinity of the $\overline{\Gamma}_{\overline{1}0}$ point. Two bands, labeled S1 and S2 in Fig. 3(a), are degenerate at the band top at $\overline{\Gamma}$, which we find experimentally to be located just below E_F. These states disperse downwards away from the band top with distinct slopes. In comparison to calculations [S1 and S2 in Fig. 2(a)] we thus assign these as the σ-band surface states of the B-terminated surface.

The π state associated with the same surface boron layer [S3 in Fig. 2(a)] is also visible experimentally in Fig. 3(a) as a band with a local maximum at the $\overline{\mathrm{M}}$ point, clearly visible along the $\overline{\Gamma}_{\overline{1}0} - \overline{\mathrm{M}} - \overline{\Gamma}_{00}$ line. The relevant band can be traced throughout momentum space, and is seen to disperse upwards to cross the Fermi level in the vicinity of the $\overline{\mathrm{K}}$ point. This gives rise to triangular Fermi pockets around the Brillouin zone corners ($\overline{\mathrm{K}}$ points) visible in Fermi surface measurements shown in Fig. 3(b). Similar features, together with similar momentum-dependent matrix element variations, were observed for the Dirac states in graphene [24], providing further evidence for the assignment of S3 as the π state of the B-terminated surface. The associated Dirac point is thus located above the Fermi level.

An additional hole band is visible at the $\overline{\Gamma}_{\overline{1}0}$ point in Fig. 3(a), labeled as S5. It appears as a copy of S1, but located at a binding energy higher by approximately 0.6 eV. We attribute this to be a surface σ-type state originating from the subsurface B layers on the Al-terminated surface, consistent with the trends of our DFT calculations shown in Fig. 2(d). Signatures of S5 can also be traced through the Brillouin zone, allowing us to assign the two band tops seen experimentally along the $\overline{\mathrm{K}}$-$\overline{\mathrm{M}}$-$\overline{\mathrm{K}}$ direction as S1 and S5 for the states with lower and higher binding energy, respectively.

Finally, we observe an electron-like pocket (labelled S4) around the $\overline{\Gamma}_{00}$ point, whose band bottom is located at -2 eV. Our Fermi surface measurements [Fig. 3(b)] reveal that this pocket gives rise to a circular Fermi surface centered around the $\overline{\Gamma}$-point. This band appears to match S4, the Al-derived surface state characteristic of the Al-terminated surface in our calculations [Fig. 2(c)]. A similar state was reported in previous ARPES studies on both MgB$_2$ [25] and AlB$_2$ [26], and in both cases it was interpreted as a surface state. It is, however, significantly broader than the other features we identify as surface states above. Moreover, in AlB$_2$, the assignment from DFT calculations is not unique, as the calculated bulk electronic structure also predicts an electron pocket around the Γ point of the bulk zone [Fig. 1(c)]. Measurements of the out-of-plane dispersion are thus necessary to uniquely determine the origin of the experimentally observed electron pocket. Similarly for the surface σ bands, we note that the bulk σ states are also expected to have a band top at the Γ point. Since all bulk states in AlB$_2$ are expected to have a nonnegligible out-of-plane dispersion [Fig. 1(c)], all observed two-dimensional states can be identified as surface states. This motivates photon energy-dependent measurements, probing

the out-of-plane dispersions, to fully disentangle the surface and bulk contributions to the measured electronic structure, as discussed below.

B. Out-of-plane dispersion

Variable photon energy measurements can be employed to determine whether a state disperses in three dimensions, as the conservation of energy and in-plane momentum in the photoemission process ensure that different photon energies probe different out-of-plane momenta k_z [16,27]. Due to the surface-sensitivity of ARPES, the out-of-plane momentum is not well defined, and each ARPES experiment is probing a range of k_z values. Nonetheless, such experiments can readily distinguish two-dimensional (2D) states, which are observed at the same binding energy regardless of the photon energy used, from three-dimensional (3D) states which disperse. To estimate the mean value of k_z corresponding to a given combination of photon energy, in-plane momentum, and binding energy, we assume a standard free-electron final state model, where the final-state dispersion is given by

$$E_{\mathrm{F}} = (\hbar^2/2m_e)(\vec{k} + \vec{G})^2 - V_0 + W, \qquad (1)$$

with m_e denoting the free electron mass, $\vec{k}$ the total electron momentum, $\vec{G}$ a reciprocal lattice vector, W the work function, and V_0 the so-called inner potential, which corresponds to the bottom of the final-state free-electron band referenced to the vacuum level [16,27]. The inner potential is a free parameter, which we estimate to be $V_0 = 19$ eV based on the periodicity of the experimental features (to be discussed in the following subsection), as well as comparisons to DFT calculations [Fig. 1(c)]. This is slightly larger than the value used to describe the measurements in MgB$_2$, $V_0 = 15$ eV [28], likely reflecting different binding energies of electrons in the two materials.

1. Boron σ states

First we concentrate on the σ states whose band top is observed at the $\overline{\Gamma}_{\overline{1}0}$ point [Fig. 3(a)]. In Fig. 4(a), we show the photoemission intensity at this in-plane momentum point, as a function of binding energy and of the out-of-plane momentum k_z, determined using Eq. (1). Three distinct states can be seen. Two of them, at the binding energies of the band tops of the S2 and S5 states identified in Fig. 3(a), are well defined and show no k_z-dispersion. This is consistent with our above assignment of S2 and S5 as surface states of a surface B layer of a B-terminated surface, and of a subsurface B layer of an Al-terminated surface, respectively [29]. The energy of the third state changes as a function of k_z, and is not well defined, i.e., the state appears broad in the measurement. Both of these observations are expected of bulk states, which disperse along k_z and exhibit k_z broadening due to the surface-sensitivity of photoemission. We therefore assign this state as the bulk σ state. Along the Γ-A line probed here, we observe spectral weight in the photoemission dispersing from 1.3 to 0.6 eV below the Fermi level, $\sim$0.5 eV closer to the Fermi level than the corresponding band positions calculated for stoichiometric AlB$_2$ [Fig. 1(c)]. This is likely as a result of charge carrier doping due to Al deficiency away from the nominal AlB$_2$ composition, suggesting that the off-stoichiometry introduces
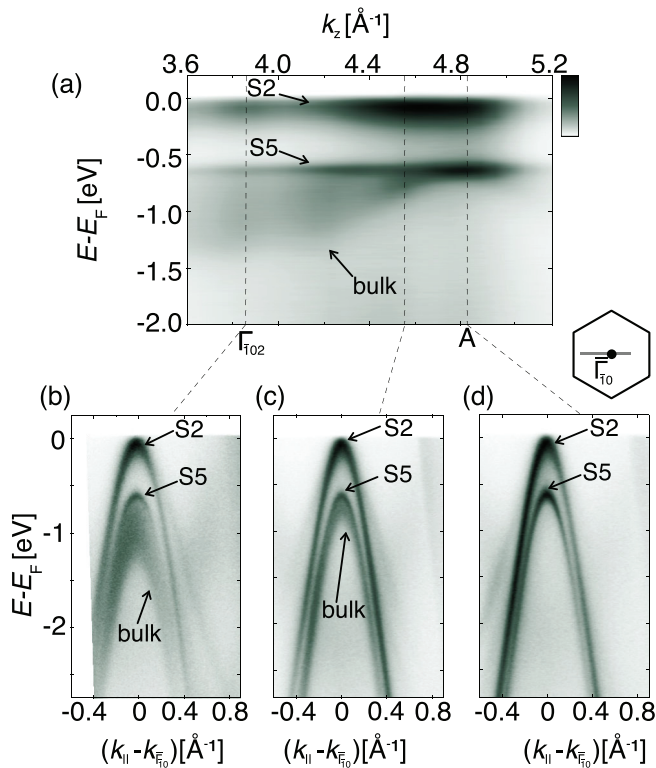
FIG. 4. (a) Out-of-plane dispersion of AlB$_2$, integrated over $k_\parallel = k_{\Gamma_{\bar{1}0}} \pm 0.1$Å. k_z was estimated assuming free-electron like final states, with an inner potential of $V_0 = 19$ eV. (b)–(d) The in-plane dispersion along the Γ-M direction (see inset), measured using photon energies of (b) $h\nu = 64$ eV, (c) $h\nu = 86$ eV, and (d) $h\nu = 96$ eV.

FIG. 5. (a) Intensity at the Fermi level ($E_F \pm 50$ meV) as a function of in-plane momentum along the Γ-M direction (see inset), and the out-of-plane momentum. (b)–(d) The corresponding in-plane dispersion, measured using photon energies of (b) $h\nu = 76$ eV, (c) $h\nu = 102$ eV, and (d) $h\nu = 116$ eV.

a rigid shift of the chemical potential relative to the σ band. Our observations also suggest that a previous ARPES measurement [26], which reported the band top of the σ states to be at ~ -1.5 eV, was representative of the Γ point, while the band top is actually at the A point. We note that the S5 surface state "hugs" the top of the bulk band at the A point, as is clearly observed in Figs. 4(b) to 4(d).

2. Al surface state

At first sight, the broadening of the electron-like S4 state in Figs. 3(a) and 3(b), attributed above as a surface state, may appear to be a k_z broadening, raising suspicion that it might in fact be a bulk state. To investigate this possibility, we performed photon-energy-dependent measurements around the $\bar{\Gamma}_{00}$ point. In Fig. 5(a) we show the Fermi level momentum distribution curve (MDC) of this state as a function of out-of-plane momentum. The two features observed at ± 0.8 Å^{-1} in the MDC map correspond to the two Fermi crossings of the investigated electron pocket, which we find do not disperse as a function of-out-of-plane momentum within our experimental resolution. In contrast, the Al-dominated bulk state seen in the DFT calculations around the Γ point disperses by about 10 eV between the Γ and A points. Similarly, the in-plane dispersion of this state remains the same regardless of the probing photon energy [Figs. 5(b) to 5(d)]. Together, these measurements unambiguously demonstrate that the state S4 is two-dimensional, confirming its assignment as the Al-derived surface state of the Al-terminated surface.
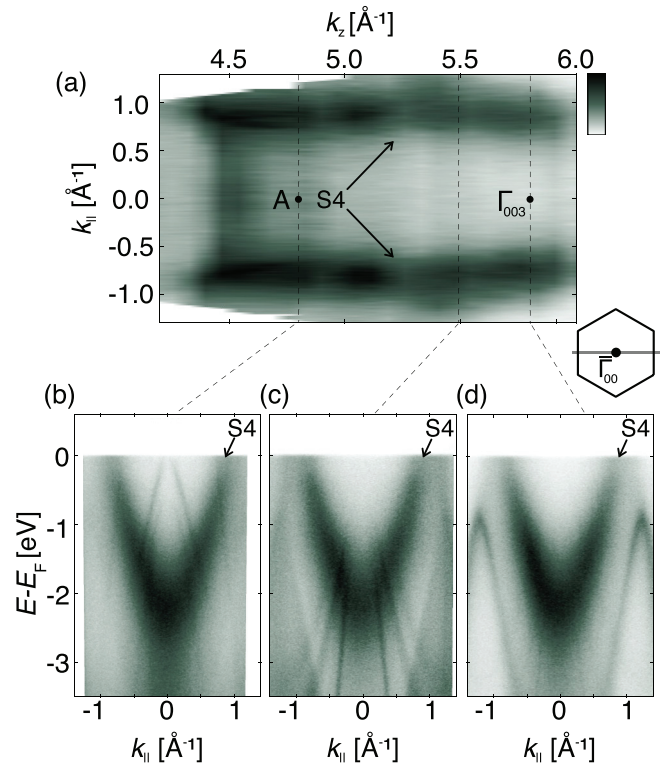
Since the evident broadening of this state can thus not be attributed to k_z broadening, we speculate that the dominant cause of its large linewidth is disorder. The fact that the surface state originating from the Al-terminated surface is broader than the ones originating from the B-terminated surface indicates that the Al-terminated surface is more disordered, likely a result of the intrinsic off-stoichiometry of the Al layer.

V. DISCUSSION

A key goal of this work was to examine whether the bulk and/or the surface boron σ states in Al$_{1-\delta}$B$_2$ either cross the Fermi level, or are close enough for external perturbations to push them across it. Our results presented above show that the bulk σ states are fully occupied, with their band top 0.6 eV below the Fermi level. This is approximately half the binding energy of these states predicted from DFT calculations for the stoichiometric compound, indicating that the off-stoichiometry of the real material has a significant impact on its electronic structure. Nonetheless, the binding energy of the bulk σ states is still sufficiently large for the external perturbations to be unlikely to drive those states across the Fermi level. While this may be achievable by deliberate doping, for example, making the bulk compound about twice as Al-deficient, it remains to be seen whether this could be done without introducing significant disorder to the boron layers.

The σ states originating from the B-terminated surface [S1 and S2 in Fig. 3(a)], on the other hand, are much closer
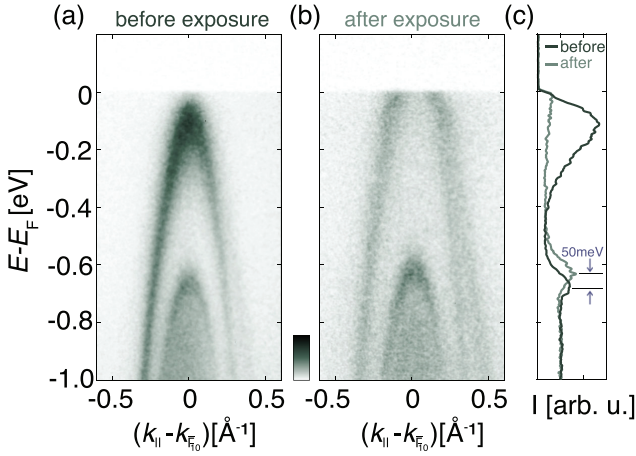
FIG. 6. The in-plane dispersion along the Γ-M direction ($h\nu =$ 66 eV), measured on (a) a pristine surface cleaved in ultra-high vacuum (10^{-11} mbar) and (b) after five minutes of exposure to a higher pressure of 10^{-8} mbar. (c) Energy distribution curves (EDCs) integrated over $k_{\|} = k_{\Gamma_{\bar{1}0}} \pm 0.05$ Å, extracted from (a), (b).

to the Fermi level. From fits to EDCs extracted from our measured dispersions [Figs. 4(b) to 4(d) and Fig. 7 of the Appendix] we estimate the band top of the surface σ states to be only 70 meV below the Fermi level. In this case external tuning, such as electrostatic gating, could prove effective in pushing the states across the Fermi level.

As a proof of principle of such tuning, we exposed the *in situ* UHV (10^{-11} mbar) cleaved clean surface of an $Al_{1-\delta}B_2$ sample to the residual rest gases in a load lock chamber, where the pressure is roughly 1000 times higher (10^{-8} mbar). We compare the σ state dispersion measured on the pristine surface [Fig. 6(a)] to that measured in UHV conditions after 5 minutes of exposure to the higher pressure [Fig. 6(b)]. The difference between the two measurements is striking. The Fermi level has clearly shifted following the exposure, resulting in the B-terminated surface boron states (S2) crossing the Fermi level, while the subsurface boron state (S5) is observed about 50 meV closer to it [Fig. 6(c)]. Moreover, the B-terminated surface states which cross the Fermi level now exhibit a sudden change of the dispersion slope ~70 meV below the Fermi level, with a decreased velocity at E_F. This is indicative of electron-phonon coupling, which is known to lead to such pronounced "kinks" in the measured σ-band dispersions in the superconducting sister compound MgB_2, in which the σ-states cross the Fermi level [30].

The observation reported in Fig. 6 motivates two types of future experiments. The first is a careful study of the influence of dosing different gases on the surface of $Al_{1-\delta}B_2$ in UHV. As well as elucidating the relevant surface chemistry which mediates the observed surface hole doping, such experiments would provide routes to control the doping level, and thus to investigate the dependence of the electron-phonon coupling strength on the occupation of the σ bands. The second is investigating the influence of other external perturbations on the surface band structure of $Al_{1-\delta}B_2$. An interesting example is in-plane uniaxial pressure, which has recently become possible to apply *in situ* together with ARPES experiments [31–33]. The lowering of symmetry caused by the uniaxial

pressure would break the degeneracy of the two σ states at the Γ point, potentially driving one of them across the Fermi level. With an appropriate uniaxial strain apparatus [34] the occupation of that band could be continuously tuned in a clean way. Each of these experiments would offer a new knob to study the electron-phonon coupling of σ bands in graphene-like structures as a function of band filling. It may even be possible to utilize such tuning parameters to drive the B-terminated surface of $Al_{1-\delta}B_2$ into a superconducting state. If achieved, this would provide an ideal model system in which to study the interplay of carrier concentration, electron-phonon coupling and superconductivity in a 2D system.

VI. CONCLUSION

We utilized angle-resolved photoemission and density functional theory to perform a comprehensive study of the surface and bulk electronic structure of aluminium diboride, with special emphasis on the binding energy of the surface and bulk boron σ bands. Our results indicate that the band top of the bulk bands is about two times closer to the Fermi level in the real material $Al_{1-\delta}B_2$ than is predicted for the stoichiometric composition AlB_2. Nonetheless, its binding energy of 600 meV is too large to expect that external tuning parameters could push the bulk bands across the Fermi level. In contrast, the surface σ states are found only 70 meV away from the Fermi level. We showed how they can be tuned across it by surface hole-doping, motivating future targeted studies aimed at controllably manipulating the surface doping of the σ-band surface states, to guide the search for possible novel surface superconductivity in this system.

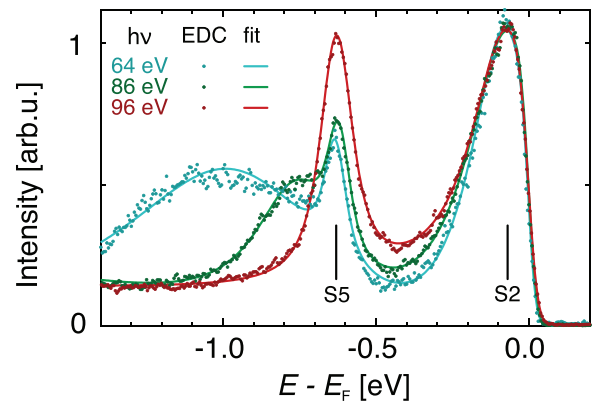The research data supporting this publication can be accessed at Ref. [35].

FIG. 7. Energy distribution curves (dots) extracted at the $\Gamma_{\bar{1}0}$ point from Figs. 4(b) to 4(d), corresponding to the measurements taken with the photon energies of 64, 86, and 96 eV, respectively. The lines are fits of two (96 eV) or three (64 and 86 eV) Lorentzian curves, convolved with the Fermi function and a Gaussian accounting for experimental resolution.

APPENDIX: ENERGY DISTRIBUTION CURVES

Here we show fits to the energy distribution curves extracted at the $\Gamma_{\bar{1}0}$ point from Figs. 4(b) to 4(d), as well as the fits to them (Fig. 7). Well-defined peaks corresponding to the surface states S2 and S5 are clearly resolved in the measurements taken using all three photon energies, with binding energies of (70 ± 5) meV and (625 ± 5) meV, respectively. Additional bulk states are seen in measurements taken using 64 and 86 eV [Figs. 4(b) and 4(c)]; we account for them in the fit using an additional Lorentzian peak.

[1] C. Buzea and T. Yamashita, Review of the superconducting properties of MgB$_2$, Supercond. Sci. Technol. **14**, R115 (2001).

[2] H. J. Choi, D. Roundy, H. Sun, M. L. Cohen, and S. G. Louie, The origin of the anomalous superconducting properties of MgB$_2$, Nature **418**, 758 (2002).

[3] I. Loa, K. Kunc, K. Syassen, and P. Bouvier, Crystal structure and lattice dynamics of AlB$_2$ under pressure and implications for MgB$_2$, Phys. Rev. B **66**, 134101 (2002).

[4] U. Burkhardt, V. Gurin, F. Haarmann, H. Borrmann, W. Schnelle, A. Yaresko, and Y. Grin, On the electronic and structural properties of aluminum diboride Al$_{0.9}$B$_2$, J. Solid State Chem. **177**, 389 (2004).

[5] H. Rosner, D. Milosavljević, K. Koch, U. Burkhardt, and Yu. Grin (unpublished).

[6] D. Sharma, J. Kumar, A. Vajpayee, R. Kumar, P. K. Ahluwalia, and V. P. S. Awana, Comparative experimental and density functional theory (DFT) study of the physical properties of MgB$_2$ and AlB$_2$, J. Supercond. Novel Magn. **24**, 1925 (2011).

[7] A. Steppke, L. Zhao, M. E. Barber, T. Scaffidi, F. Jerzembeck, H. Rosner, A. S. Gibbs, Y. Maeno, S. H. Simon, A. P. Mackenzie, and C. W. Hicks, Strong peak in T$_c$ of Sr$_2$RuO$_4$ under uniaxial pressure, Science **355**, eaaf9398 (2017).

[8] Q. Chen, J. Stajic, S. Tan, and K. Levin, BCS–BEC crossover: From high temperature superconductors to ultracold superfluids, Phys. Rep. **412**, 1 (2005).

[9] M. Randeria and E. Taylor, Crossover from Bardeen-Cooper-Schrieffer to Bose-Einstein condensation and the unitary fermi gas, Annu. Rev. Condens. Matter Phys. **5**, 209 (2014).

[10] C. Noguera, Polar oxide surfaces, J. Phys.: Condens. Matter **12**, R367 (2000).

[11] M. A. Hossain, J. D. F. Mottershead, D. Fournier, A. Bostwick, J. L. McChesney, E. Rotenberg, R. Liang, W. N. Hardy, G. A. Sawatzky, I. S. Elfimov, D. A. Bonn, and A. Damascelli, *In situ* doping control of the surface of high-temperature superconductors, Nat. Phys. **4**, 527 (2008).

[12] Z.-H. Zhu, A. Nicolaou, G. Levy, N. P. Butch, P. Syers, X. F. Wang, J. Paglione, G. A. Sawatzky, I. S. Elfimov, and A. Damascelli, Polarity-Driven Surface Metallicity in SmB$_6$, Phys. Rev. Lett. **111**, 216402 (2013).

[13] V. Sunko, H. Rosner, P. Kushwaha, S. Khim, F. Mazzola, L. Bawden, O. J. Clark, J. M. Riley, D. Kasinathan, M. W. Haverkort, T. K. Kim, M. Hoesch, J. Fujii, I. Vobornik, A. P. Mackenzie, and P. D. C. King, Maximal Rashba-like spin splitting via kinetic-energy-coupled inversion-symmetry breaking, Nature **549**, 492 (2017).

[14] F. Mazzola, V. Sunko, S. Khim, H. Rosner, P. Kushwaha, O. J. Clark, L. Bawden, I. Marković, T. K. Kim, M. Hoesch, A. P. Mackenzie, and P. D. C. King, Itinerant ferromagnetism of the Pd-terminated polar surface of PdCoO$_2$, Proc. Natl. Acad. Sci. USA **115**, 12956 (2018).

[15] Y. Zhao, C. Lian, S. Zeng, Z. Dai, S. Meng, and J. Ni, Two-gap and three-gap superconductivity in AlB$_2$-based films, Phys. Rev. B **100**, 094516 (2019).

[16] S. Hufner, *Photoelectron Spectroscopy*, Advanced Texts in Physics (Springer, Berlin, 2003).

[17] M. Hoesch, T. K. Kim, P. Dudin, H. Wang, S. Scott, P. Harris, S. Patel, M. Matthews, D. Hawkins, S. G. Alcock, T. Richter, J. J. Mudd, M. Basham, L. Pratt, P. Leicester, E. C. Longhi, A. Tamai, and F. Baumberger, A facility for the analysis of the electronic structures of solids and their surfaces by synchrotron radiation photoelectron spectroscopy, Rev. Sci. Instrum. **88**, 013106 (2017).

[18] K. Koepernik and H. Eschrig, Full-potential nonorthogonal local-orbital minimum-basis band-structure scheme, Phys. Rev. B **59**, 1743 (1999).

[19] J. P. Perdew and Y. Wang, Accurate and simple analytic representation of the electron-gas correlation energy, Phys. Rev. B **45**, 13244 (1992).

[20] J. P. Perdew, K. Burke, and M. Ernzerhof, Generalized Gradient Approximation Made Simple, Phys. Rev. Lett. **77**, 3865 (1996).

[21] J. M. An and W. E. Pickett, Superconductivity of MgB$_2$: Covalent Bonds Driven Metallic, Phys. Rev. Lett. **86**, 4366 (2001).

[22] D. Takane, S. Souma, K. Nakayama, T. Nakamura, H. Oinuma, K. Hori, K. Horiba, H. Kumigashira, N. Kimura, T. Takahashi, and T. Sato, Observation of a Dirac nodal line in AlB$_2$, Phys. Rev. B **98**, 041105(R) (2018).

[23] F. Mazzola, T. Frederiksen, T. Balasubramanian, P. Hofmann, B. Hellsing, and J. W. Wells, Strong electron-phonon coupling in the σ band of graphene, Phys. Rev. B **95**, 075430 (2017).

[24] A. Bostwick, T. Ohta, T. Seyller, K. Horn, and E. Rotenberg, Quasiparticle dynamics in graphene, Nat. Phys. **3**, 36 (2007).

[25] H. Uchiyama, K. M. Shen, S. Lee, A. Damascelli, D. H. Lu, D. L. Feng, Z.-X. Shen, and S. Tajima, Electronic Structure of MgB$_2$ from Angle-Resolved Photoemission Spectroscopy, Phys. Rev. Lett. **88**, 157002 (2002).

[26] S. Souma, T. Sato, T. Takahashi, N. Kimura, and H. Aoki, Electronic band structure of AlB$_2$ studied by angle-resolved photoemission spectroscopy, J. Electron Spectrosc. Relat. Phenom. **144–147**, 545 (2005).

[27] A. Damascelli, Probing the electronic structure of complex systems by ARPES, Phys. Scr. **T109**, 61 (2004).

[28] Y. Sassa, M. Månsson, M. Kobayashi, O. Götberg, V. N. Strocov, T. Schmitt, N. D. Zhigadlo, O. Tjernberg, and B. Batlogg, Probing two- and three-dimensional electrons in MgB_2 with soft x-ray angle-resolved photoemission, Phys. Rev. B **91**, 045114 (2015).

[29] We note that S1 is degenerate with S2 at the $\overline{\Gamma}$ point shown here, and thus the assignment of S1 as a surface state is equally supported by these photon energy-dependent measurements.

[30] D. Mou, R. Jiang, V. Taufour, R. Flint, S. L. Bud'ko, P. C. Canfield, J. S. Wen, Z. J. Xu, G. Gu, and A. Kaminski, Strong interaction between electrons and collective excitations in the multiband superconductor MgB_2, Phys. Rev. B **91**, 140502(R) (2015).

[31] S. Riccò, M. Kim, A. Tamai, S. M. Walker, F. Y. Bruno, I. Cucchi, E. Cappelli, C. Besnard, T. K. Kim, P. Dudin, M. Hoesch, M. J. Gutmann, A. Georges, R. S. Perry, and F. Baumberger, *In situ* strain tuning of the metal-insulator-transition of Ca_2RuO_4 in angle-resolved photoemission experiments, Nat. Commun. **9**, 1 (2018).

[32] H. Pfau, C. R. Rotundu, J. C. Palmstrom, S. D. Chen, M. Hashimoto, D. Lu, A. F. Kemper, I. R. Fisher, and Z.-X. Shen, Detailed band structure of twinned and detwinned $BaFe_2As_2$ studied with angle-resolved photoemission spectroscopy, Phys. Rev. B **99**, 035118 (2019).

[33] V. Sunko, E. A. Morales, I. Marković, M. E. Barber, D. Milosavljević, F. Mazzola, D. A. Sokolov, N. Kikugawa, C. Cacho, P. Dudin, H. Rosner, C. W. Hicks, P. D. C. King, and A. P. Mackenzie, Direct observation of a uniaxial stress-driven Lifshitz transition in Sr_2RuO_4, npj Quantum Mater. **4**, 46 (2019).

[34] C. Hicks, M. E. Barber, S. D. Edkins, D. O. Brodsky, and A. P. Mackenzie, Piezoelectric-based apparatus for strain tuning, Rev. Sci. Instrum. **85**, 065003 (2014).

[35] https://doi.org/10.17630/024966a8-67e1-4270-96fe-2f4bd51bea8b.